Periodic forcing and feedback control of nonlinear lumped oscillators and meandering spiral waves

V S. Zykov, G. Bordiougov, H. Brandtstädter, I. Gerdes, and H. Engel
Institut für Theoretische Physik, Technische Universität Berlin, Hardenbergstrasse 36, D-10623 Berlin, Germany
(Received 8 April 2003; published 16 July 2003)

It is shown that meandering spiral waves rotating in excitable media subjected to periodic external forcing or feedback control resemble many features of nonlinear lumped oscillators. In particular, the period shift function obtained for the Poincaré oscillator is qualitatively identical to that for spiral waves under fixed phase control. On the other hand, under one-channel feedback control, meandering spiral waves exhibit quite different dynamic regimes appearing as specific features of a distributed system. In particular, three types of attractors (resonance, entrainment, and asynchronous) of spiral waves are observed in experiments with the light-sensitive Belousov-Zhabotinsky reaction and in numerical simulations performed for the underlying Oregonator model. A theory of the resonance attractor for meandering spiral waves is developed which predicts the attractor radius and specifies the basins of attraction in good quantitative agreement with the numerical computations and experimental observations.

DOI: 10.1103/PhysRevE.68.016214 PACS number(s): 05.45.−a, 05.65.+b, 82.40.Bj, 47.54.+r

I. INTRODUCTION

Nonlinear oscillators subjected to external forcing exhibit very rich dynamics and are intensively studied in application to many objects in physics, chemistry, and biology [1–6]. Meandering spiral waves rotating in distributed excitable media resemble basic features of nonlinear oscillators and, in particular, can be synchronized by application of a periodic parametric modulation [7,8]. However, the distributed nature of excitable media allows us also to observe quite different dynamical regimes, such as a resonance drift of spirals induced by external forcing [9,10]. Moreover, feedback-controlled forcing of an excitable medium creates conditions for the formation of so-called resonance and entrainment attractors of spiral waves [11,12].

The controlled dynamics of spiral waves induced by a modulation of the excitability is important for many applications, e.g., for the defibrillation of cardiac tissue [13,14]. In this connection, theoretical and experimental investigations of parametrically forced spiral waves are a subject of growing interest [15–22]. However, the theory of the resonance attractor of spiral waves is up to now elaborated only in application to rigidly rotating spirals [17,21,22], while it was first discovered in experiments with meandering spirals [11]. Recent results [18] arouse a hope that the existing theory can be generalized to the case of meandering spiral waves.

In this paper, we perform a systematic numerical and experimental study of meandering spiral waves subjected to external stimulation and develop on this basis the appropriate theoretical description. In the first part of the paper, a periodic forcing and a feedback control of the Poincaré oscillator is considered in order to illustrate some general properties of lumped nonlinear oscillators. Then, periodic forcing and fixed phase feedback control of meandering spiral waves are studied in the Oregonator model. The next part is devoted to a description of spiral wave dynamics in the Oregonator model subjected to a one-channel feedback. Here a theory of the resonance attractor of meandering spiral waves is presented. After this, the experimental results obtained for the light-sensitive Belousov-Zhabotinsky (BZ) reaction are described. In the final part, the theoretical and the experimental data presented in the paper are discussed.

II. POINCARÉ OSCILLATOR

The Poincaré oscillator is commonly used in order to capture important qualitative features of nonlinear oscillators under external forcing [3,23]. It is convenient to express the corresponding evolution equations in a polar coordinate system (r,θ):

$$\frac{dr}{dt}=kr(1-r), \tag{1}$$

$$\frac{d\theta}{dt}=2\pi.$$

Starting at $r=1$, the phase point will describe the unit circle with monotonously increasing θ. The system achieves this attractor starting at any value of r, except $r=0$. The parameter k determines the rate at which the value of r approaches $r=1$. The phase of the established oscillation is naturally specified by the polar angle θ.

We consider first the dynamics of the Poincaré oscillator under a periodic sequence of short pulses. Let us assume that each of these pulses forces a jump of the point from (x,y) to $(x',y')=(x,y+a)$, where (x,y) are Cartesian coordinates. Of course, such a jump changes the momentary radius r_i to the new value

$$r_i'=\sqrt{r_i^2+a^2+2r_ia\sin\theta_i}, \tag{2}$$

where θ_i is the phase just before the ith pulse was applied.

The pulse induces also a phase shift ϑ_i that can be found from the equation

$$\cos\vartheta_i=\frac{r_i+a\sin\theta_i}{\sqrt{r_i^2+a^2+2r_ia\sin\theta_i}}. \tag{3}$$

In the limit $k\to\infty$, the disturbed value of r_i' immediately approaches the unit circle. In this case, the effect of periodic forcing on the Poincaré oscillator is completely determined by a one-dimensional map

$$\theta_{i+1}=\theta_i+\vartheta_i+2\pi T, \tag{4}$$

where T is the stimulation period that can differ from the natural period $T_e=1$.

In the regime of a one-to-one frequency synchronization, two equalities are valid: $\theta_{i+1}=\theta_i+2\pi$ and $\vartheta_i=\vartheta_{i+1}=\vartheta$. Then, from Eq. (4) follows the condition for the synchronization:

$$T=1-\frac{\vartheta}{2\pi}. \tag{5}$$

Substitution of Eq. (3) with $r=1$ into Eq. (5) gives a relationship between the locking angle θ and and the shifted period (i.e., the forcing period) T in the synchronized regime:

$$T=1-\frac{1}{2\pi}\arccos\left(\frac{1+a\sin\theta}{\sqrt{1+a^2+2a\sin\theta}}\right). \tag{6}$$

Such a relationship is called the period shift function [24]. In the case of small perturbations $a\ll 1$, its analytical expression becomes very simple:

$$T=1-\frac{a\cos\theta}{2\pi}. \tag{7}$$

This pure harmonic shape of the period shift function is a very general property of nonlinear oscillators under small perturbations [24].

Note, that the locking angle θ specifies the phase shift between the oscillations and the external forcing. In experiments with oscillating systems, it is suitable to characterize this phase shift by a time delay τ between some marker event and the application of a perturbation.

In Fig. 1(a), the period shift function computed for $k=5$ and $a=0.5$ is plotted using $\tau=\theta/(2\pi)$ as an independent variable. The obtained shape of the period shift function deviates only slightly from the harmonic limit (7). Synchronization (frequency locking) is restricted to a certain interval of the external period T. Outside of this entrainment band, quasiperiodic oscillations occur [1]. For each value of T within the entrainment band, there are two synchronized regimes corresponding to quite different values of the time delay τ [see Fig. 1(a)]. However, a linear stability analysis of map (4) reveals that only those regimes are stable for which $d\vartheta/d\theta<0$. Taking into account Eq. (5), it gives the following stability condition:

$$\frac{dT}{d\tau}>0. \tag{8}$$

Direct integration of the Poincaré model (1) subjected to a periodic forcing confirms this analytical prediction: synchronized oscillations are possible only on the branches of the period shift function with positive slope [see diamonds in Fig. 1(a)].

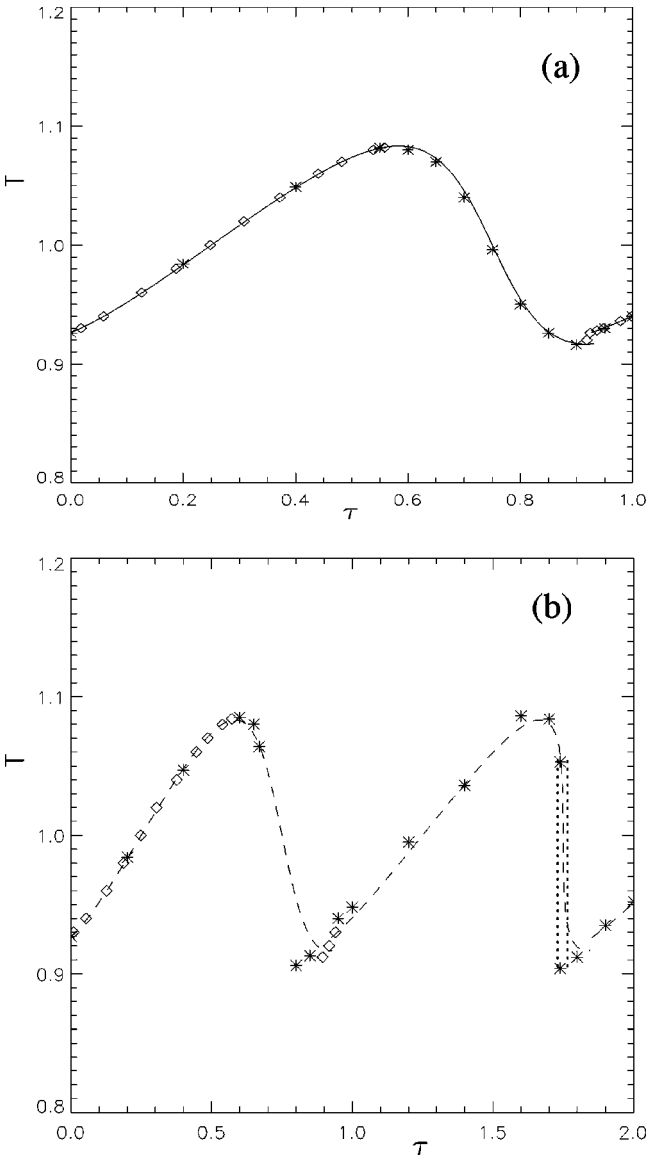

FIG. 1. Period shift function computed for the Poincaré oscillator (1). (a) The solid curve corresponds to the analytical expression (6) with $\tau=\theta/(2\pi)$. Diamonds and asterisks are obtained from direct integration of Eq. (1) with $k=5$ under periodic forcing and feedback control, respectively. (b) The dashed curve shows the period shift function extrapolated until $\tau=2$. Diamonds and asterisks represent results of direct integration of (1) with $k=2$ under periodic forcing and feedback control, correspondingly. Dotted lines indicate the bistability interval.

It is important to compare these results with feedback-controlled forcing of the Poincaré oscillator. As an example, let us consider the following feedback mechanism, which is called fixed phase feedback control [25]. Here the forcing pulses are applied with a fixed time delay τ after the instant when $\theta=0$. Hence, all perturbations will be applied at the same phase $\theta=2\pi\tau$. In the case $k\to\infty$, the phase point returns immediately to the limit cycle. Thus, after the very first

pulse has been applied, a periodic regime will be established with a period T depending on the value of τ as specified by the period shift function (6). Obviously, under the feedback control, all branches of this function are stable, if k is infinitely large.

Direct integration of model (1) subjected to the fixed phase feedback control demonstrates that all periodic regimes determined by the period shift function can remain stable even for finite values of k. Figure 1(a) illustrates such a possibility for $k=5$. Thus, the feedback control reveals some branches of the period shift function, which are impossible to observe under periodic forcing. Moreover, by application of the feedback control, the boundaries of the entrainment band (Arnold tongue) are determined much more easily than by periodic forcing. For each value of τ, periodic oscillations are established very quickly, and it is not necessary to integrate Eq. (1) during a long time in order to distinguish pure periodic from quasiperiodic regimes as it should be done in the case of periodic forcing.

However, if the rate constant k becomes smaller, the system has no time to return back to the unit circle after a perturbation and the history of the previous stimulations should be taken into account. Let r_i and θ_i be the values of r and θ just before the ith perturbation. Then the value of r_i' after the perturbation obeys Eq. (2) and the phase jump ϑ_i is specified by Eq. (3). This phase jump determines a time T_i until the next perturbation:

$$T_i = 1 - \frac{\vartheta_i}{2\pi}, \tag{9}$$

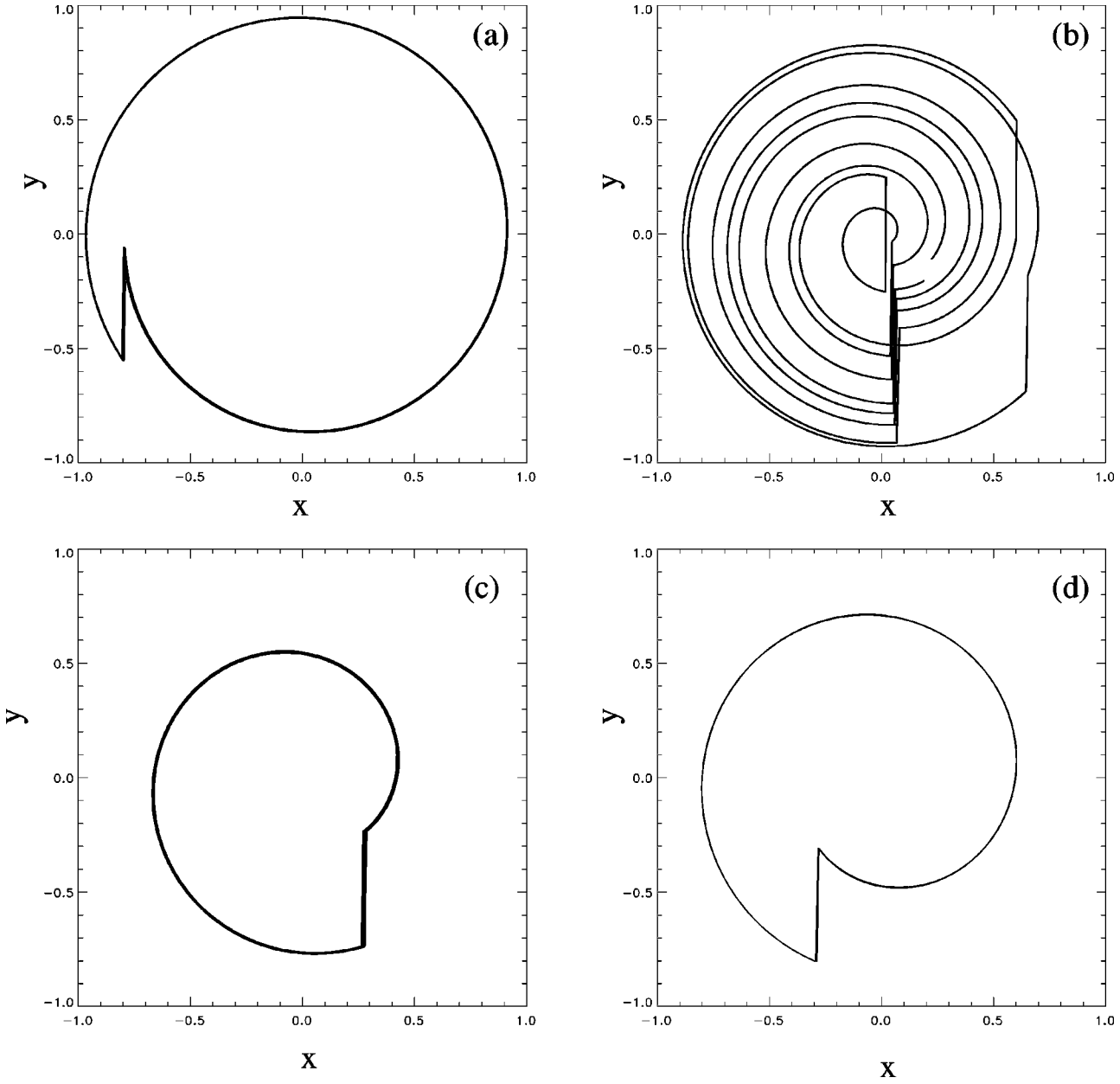

FIG. 2. Trajectories of the Poincaré oscillator (1) subjected to the feedback control computed for $k=2$ and different values of the time delay. (a) $\tau=0.6$, (b) $\tau=0.76$, (c) and (d) $\tau=1.74$.

which is not necessarily constant in contrast to the case of the periodic forcing.

The value r_{i+1} just before the $(i+1)$th perturbation can be found by integration of the system (1) [25], which gives

$$r_{i+1}=\frac{r_i'}{r_i'-(r_i'-1)\exp(-kT_i)}. \tag{10}$$

The stationary state $r_p=r_i=r_{i+1}$ of maps (2), (3), (9), and (10) determines possible periodic regimes of the Poincaré oscillator under the feedback control. These regimes are stable for

$$\left|\frac{dr_{i+1}}{dr_i}\right|_{r_i=r_p}<1. \tag{11}$$

The derivative dr_{i+1}/dr_i vanishes when $k\to\infty$ and remains small enough for $k=5$. This explains the stability of the synchronized regimes shown in Fig. 1(a) by asterisks.

However, direct integration of Eq. (1) performed for $k=2$ demonstrates that not all periodic regimes induced by the feedback are necessarily stable, since condition (11) is not valid for some values of τ. For instance, Fig. 2(a) shows a stable periodic trajectory of system (1) computed for $\tau=0.6$, while the computations for $\tau=0.76$ lead to an unclosed irregular trajectory shown in Fig. 2(b). This trajectory appears due to an instability of the periodic oscillations corresponding to this value of the time delay.

Another interesting feature of the feedback-controlled Poincaré oscillator is a bistability phenomenon that can be observed for relatively long time delay. To consider this situation, the period shift function shown in Fig. 1(a) can be easily extrapolated to an arbitrary large value of the time delay. Indeed, if periodic oscillations occur at the time delay τ with the oscillation period $T=T(\tau)$, then the same periodic regime should be observed at the time delay $\tau+T(\tau)$. The extrapolated phase shift function obtained after such a transformation is shown in Fig. 1(b) by the dashed curve. Obviously, this transformation flattens branches with a positive slope and enhances negative slopes. In particular, the slope of the period shift function near $\tau=1.75$ becomes practically vertical. At the time delay $\tau=2.75$, the slope is even positive, and the period shift function becomes bistable [not shown in Fig. 1(a)].

This bistability can also be observed for shorter time delay, if the rate constant k becomes smaller. Note that the dashed curve in Fig. 1(b) corresponds to the period shift function obtained at $k=5$, which is practically the same as for $k\to\infty$. Diamonds and asterisks in Fig. 1(b) represent periodic regimes of system (1) computed with $k=2$ for the periodic forcing and the feedback control, respectively. Data of feedback-control computations differ only slightly from the asymptotic shape of the period shift function. However, a bistability is observed near $\tau=1.74$. Figure 2(c) shows the trajectory obtained as a result of integration of system (1) with continuously increasing value of τ. Decreasing of τ starting at $\tau=2.0$ results in a quite different trajectory shown in Fig. 2(d).

The considered example of the Poincaré oscillator demonstrates that the period shift function is an appropriate tool to compare the dynamics of nonlinear oscillators subjected to periodic forcing and to feedback control. In the following sections, the obtained results and methods will be used to analyze the dynamics of meandering spiral waves in distributed excitable systems.

III. PERIODIC FORCING AND FIXED PHASE FEEDBACK CONTROL OF MEANDERING SPIRAL WAVES

Meandering spiral waves are common spatiotemporal patterns in excitable media and are intensively studied in experiments with the Belousov-Zhabotinsky reaction [3,26–28]. The two-component Oregonator model is widely used to simulate the light-sensitive version of this reaction:

$$\frac{\partial u}{\partial t}=\nabla^2 u+\frac{1}{\epsilon}\left[u-u^2-(fv+\phi)\frac{u-q}{u+q}\right],$$
$$\frac{\partial v}{\partial t}=u-v. \tag{12}$$

Here the variables u and v correspond to the concentrations of the autocatalytic species $HBrO_2$ and the catalyst, respectively. The parameters $\epsilon=0.05$, $q=0.002$, and $f=2.0$ were fixed. The term $\phi=\phi(t)$ describes the additional bromide production that is induced by the external illumination of the system [29]. In order to simulate a periodic forcing of the system, the function $\phi(t)$ is given as a sequence of impulses with amplitude $A=0.008$ and duration $D=0.3$, which are added to a background intensity $\phi_0=0.01$. The computations were performed by the explicit Euler method on a 380 $\times$380 array with a grid spacing $\Delta x=0.2$ and time steps $\Delta t=0.002$.

A spiral rotating counterclockwise near the center of the simulated domain was created by a special choice of initial conditions for system (12). The unperturbed trajectory of the spiral wave tip and the shape of the spiral are shown in Fig. 3(a).

The observed compound rotation (meandering motion) of the spiral tip can be characterized by two different periods. The oscillation period measured at the symmetry center of unperturbed trajectory was $T_0=2.8$. A different period $T_\infty=3.6$ was measured far enough from the center near the domain boundary.

Far away from the rotation center, the meandering spiral wave resembles a rigidly rotating spiral: it has the form of an Archimedean spiral and uniformly rotates at a period T_∞. Moreover, a periodic parametric forcing with the period $T=T_\infty$ induces a resonant drift of the rotation center [see Fig. 3(b)], as known for a rigidly rotating spiral [9,10].

A quite different phenomenon, namely entrainment, can be observed if the stimulation period is chosen to be close to T_0 [7]. Under such a forcing, the rotation center does not move, but the shape of the spiral tip trajectory is changed with respect to the unperturbed one. Within an entrainment

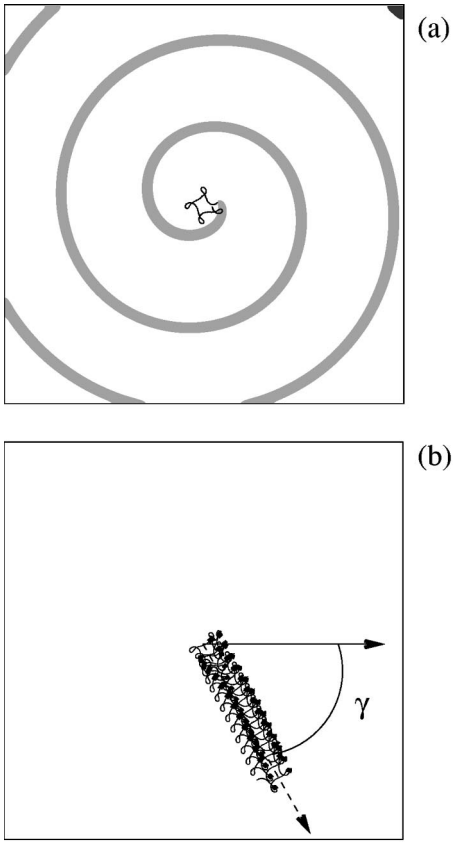

FIG. 3. Trajectory of the spiral wave tip computed from model (12). (a) The unperturbed trajectory (solid) and the momentary location of the spiral wave (shaded regions). (b) Resonant drift induced by a periodic parametric forcing with the period $T=T_\infty=3.6$. Thick segments of the trajectory correspond to applied external impulses. The drift direction is specified by angle γ.

band, the motion of the spiral tip is synchronized with the external periodic forcing, similar to the case of the Poincaré oscillator considered above. Three examples of entrained trajectories are shown in Figs. 4(a)–4(c). The number of lobes grows with the stimulation period. Of course, deformations of the trajectory shape are closely connected to variations of the phase at which the external impulses are applied.

In order to specify the phase of external forcing, let us consider the propagation velocity V of the spiral wave tip. This value oscillates at the period T_0 for the unperturbed spiral and at the period T within the synchronization band, as shown in Fig. 5. A suitable marker event in these oscillations is the instant at which the increasing velocity reaches a given value $V=V_0$. The delay τ can be determined as the time interval between this event and the application of the external pulse.

Using this definition of τ, the period shift function corresponding to the periodic forcing of the meandering spiral is specified by diamonds in Fig. 6. As in the case of the Poincaré oscillator, synchronization takes place for T within an entrainment band. However, it can be assumed that these data show only the branch of the period shift function with positive slope, because the branches with negative slope are unstable under periodic forcing.

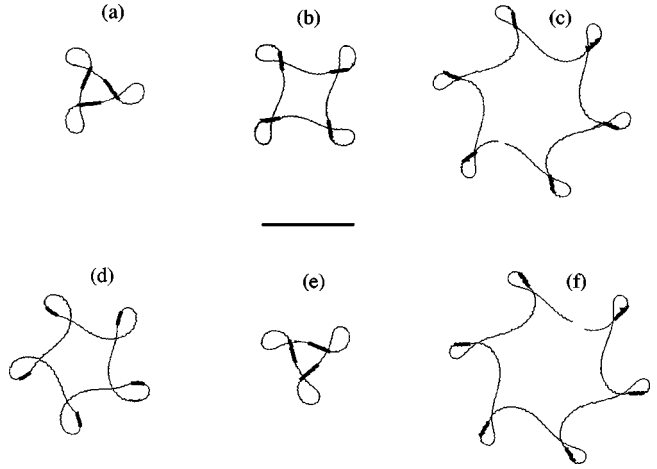

FIG. 4. Trajectories of the spiral wave tip computed for model (14) under periodic forcing at different periods (a)–(c) and under fixed phase feedback control (a)–(f). (a) $T=2.29$, $\tau=0$; (b) $T=2.68$, $\tau=0.62$; (c) $T=3.11$, $\tau=1.3$; (d) $\tau=2.0$, $T=2.84$; (e) $\tau=4.6$, $T=2.3$; (f) $\tau=4.6$, $T=3.12$. Thick segments of the trajectory correspond to the application of the external impulses. Scale bar: five Oregonator space units.

In order to show the domains with negative slope, let us apply a fixed phase control mechanism to meandering spiral waves. To this end, the pulses are generated immediately at the instance t, when $V(t)=V_0$, or after a time delay τ. Hence, all pulses are applied at the same well-defined oscillation phase. Under similar fixed phase control, the whole period shift function was reproduced in the case of the Poincaré oscillator [e.g., see Fig. 1(a)].

For the meandering spiral wave, this fixed phase feedback also gives interesting results shown in Fig. 6 by the dashed curve. During these computations, the time delay was

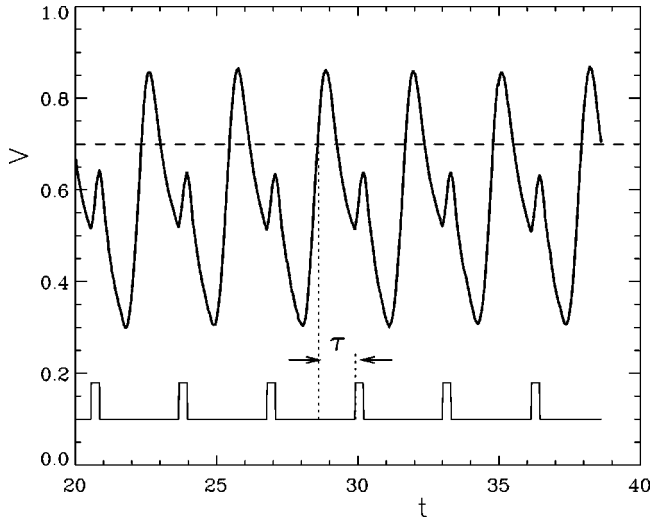

FIG. 5. Oscillations of the spiral tip velocity V corresponding to the synchronized rotation shown in Fig. 4(c). The thin solid line represents the stimulation sequence. The dashed line indicates the chosen threshold value $V_0=0.7$ (Oregonator space units per Oregonator time units). The dotted lines illustrate the definition of the time delay τ. Time t is measured in Oregonator time units.

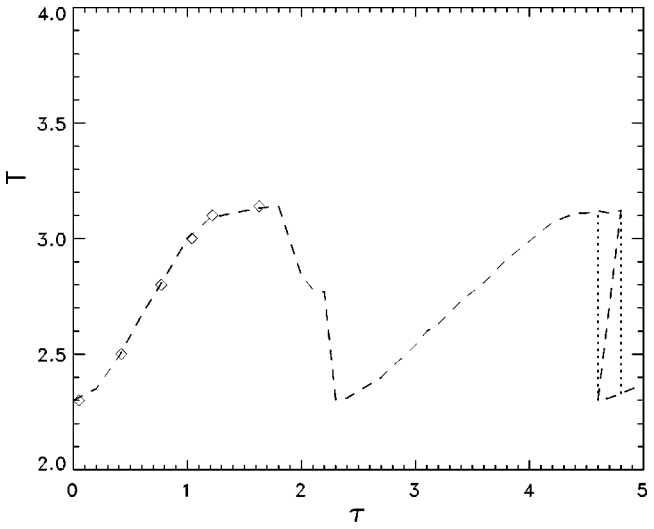

FIG. 6. Period shift function corresponding to periodic forcing (diamonds) and the fixed phase stimulation (dashed line) of the meandering spiral wave computed for the Oregonator model (12). Dotted lines indicate the bistability interval. The rotation period and time delay are measured in Oregonator time units.

changed within an interval from zero to $\tau \approx 2T_0$. At the leftmost branch of the period shift function with a positive slope, the results of the periodic stimulation completely coincide with those obtained for the fixed phase stimulation. In particular, the trajectories shown in Figs. 4(a)–4(c) are the same for both types of stimulations. However, the fixed phase control allows us to reproduce additional oscillating regimes corresponding to the branches with a negative slope. An example of such a trajectory is shown in Fig. 4(d). Here, in contrast to Figs. 4(a)–4(c), the external pulses are applied after the local curvature maxima of the trajectory have been reached. Note that the time delay in Fig. 4(d) is larger than a half of the period T_0.

The comparison of Figs. 4(a) and 4(e) illustrates the possibility to extrapolate the period shift function computed for relatively small τ to larger values using the transformation $\tau' = \tau + nT(\tau)$, where n is an integer. Indeed, the trajectory shown in Fig. 4(e) is practically identical to the one in Fig. 4(a), although the corresponding time delays differ by $2T(0)$.

Again, as in the case of the Poincaré oscillator, a bistability phenomenon is found in a narrow interval of τ restricted by the dotted lines in Fig. 6. Indeed, for the time delay $\tau = 4.6$, two quite different trajectories are observed [cf. Figs. 4(e) and 4(f)].

IV. THE OREGONATOR MODEL UNDER ONE-CHANNEL FEEDBACK

In order to realize the fixed phase control considered above, very detailed information about the spiral tip motion should be available. Usually such information is rather difficult to collect in experiments and therefore another feedback-control scheme, the so-called one-channel feedback, is applied [11]. In accordance with this scheme, the wave activity

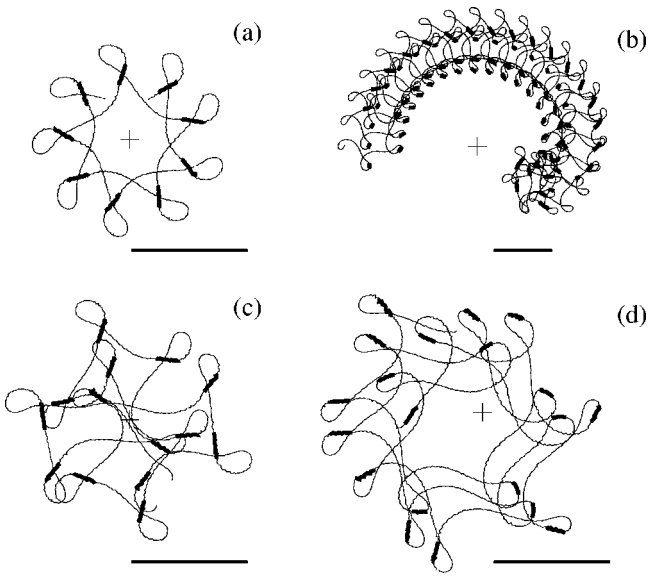

FIG. 7. Trajectories of the spiral wave tip computed for model (12) under the one-channel feedback. (a) $\tau = 0.6$, $T = 2.84$; (b) $\tau = 1.4$; (c) $\tau = 1.3$; (d) $\tau = 2.0$. Thick segments of the trajectory correspond to the application of the external impulses. Scale bar: five Oregonator space units.

(e.g., the value of the variable v) is measured at a particular detection point as a function of time. This value oscillates with time. A natural marker event in these oscillations is an instant at which the value of v exceeds a given threshold v_{th}. Consistent with the previously used definitions, the time delay τ can be specified as the time interval between this event and the application of the external pulse.

Meandering spiral waves in the Oregonator model subjected to this one-channel feedback exhibit quite different dynamics compared to the fixed phase control. In particular, the spiral dynamics depends on the distance between the detection point and the spiral wave core.

For instance, if initially the detection point is chosen rather close to the spiral wave tip, the application of the one-channel feedback leads to the so-called entrainment attractor [11,12]. The rotation center of the spiral starts to move toward the detection point, and after a transient process a perfectly synchronized trajectory of the spiral wave tip can be registered. An example of such synchronized motion computed with the Oregonator model is shown in Fig. 7(a). The same shape of the trajectory with the same oscillation period can be found in computations under fixed phase stimulation. However, it takes some time in order to achieve the synchronized motion by application of the one-channel feedback, while the fixed phase control leads to immediate synchronization. Obviously, the value of the time delays corresponding to these synchronized regimes should be different, because of the quite different definitions of the marker events.

The period shift function corresponding to computations of the entrainment attractor for different values of τ is shown by asterisks in Fig. 8. Data obtained for periodic forcing with the same definition of the time delay are shown by diamonds. These data belong to the leftmost branch of the period shift

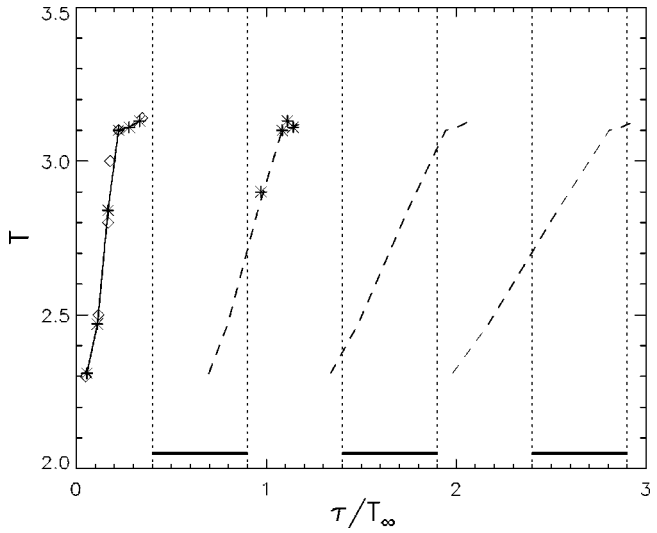

FIG. 8. Period shift function corresponding to periodic forcing (diamonds) and one-channel feedback (asterisks) computed for the Oregonator model (12). Dashed lines represent other branches of the period shift function obtained after its extrapolation to larger values of τ. Within intervals of τ bounded by dotted lines and marked by bars, the resonance attractors are observed. The rotation period is measured in Oregonator time units.

function with a positive slope, which looks qualitatively similar to that obtained above (cf. Fig. 6). This branch is extrapolated to larger values of τ by the transformation $\tau' = \tau + nT(\tau)$.

The main qualitative difference between the period shift functions shown in Figs. 6 and 8 is that under the one-channel feedback, it is not possible to obtain the branches with a negative slope. Moreover, very often it was impossible to observe synchronized motion even for branches with a positive slope.

The main reason for this discrepancy is the existence of the so-called resonance attractor of spiral waves [11,12]. A specific feature of this dynamic regime is a relatively large distance between the detection point and the spiral core center. However, the resonance attractor can be achieved even if the detection point is initially located rather close to the spiral core. This happens, for instance, if the time delay τ is chosen larger than the boundary value marked by the left dotted line in Fig. 8. Figure 7(b) illustrates the trajectory of the spiral tip computed for this case. The trajectory consists of a meandering motion of the spiral tip that resembles the unperturbed one, superimposed by a drift of the symmetry center. After a transient process, this drift occurs along a circle centered at the detection point.

While the entrainment attractor resembles synchronized oscillations of lumped systems, the resonance attractor is a typical property of a distributed medium. A theory of the resonance attractor has been elaborated recently [17,21] in application to a rigidly rotating spiral. In order to extend this theory to the case of a meandering spiral, let us assume that far away from the symmetry center the shape of a counterclockwise rotating wave front is approximated by an Archimedean spiral:

$$\Theta(r,t) = \Theta_0 - \frac{2\pi}{\lambda} r + \omega t, \tag{13}$$

where λ is the wavelength and $\omega = 2\pi/T_\infty$ is the angular velocity. The constant angle Θ_0 specifies the orientation of the spiral at $t=0$.

Periodic forcing of the spiral by a sequence of short pulses will result in a resonant drift, as shown in Fig. 3(b). To simplify considerations, each pulse will be represented as a δ function of time. Let us assume that under the periodic forcing given as $I(t) = A\delta[\cos(\omega t) - 1]$ and $\Theta_0 = 0$, the observed direction of the resonant drift is specified by an angle $\gamma = \varphi$ with respect to the X axis. For a fixed shape of the pulses, this angle is a characteristic parameter of the excitable medium. Obviously, for an arbitrary Θ_0, the drift angle will be $\gamma = \varphi + \Theta_0$. A periodic forcing in the form $I(t) = A\delta[\cos(\omega t - \phi_m) - 1]$ with a phase shift ϕ_m can be considered as a stimulation with $\phi_m = 0$, but with initial spiral orientation taken at the time $t_0 = \phi_m/\omega$. Thus, the drift direction for an arbitrary chosen Θ_0 and ϕ_m can be written as

$$\gamma = \varphi + \Theta_0 + \phi_m . \tag{14}$$

Under the one-channel feedback control, the phase of the stimulating pulse sequence depends on the spiral location. For instance, if the spiral wave center is placed at the point $(d,0)$, the spiral front specified by Eq. (13) crosses the origin of the coordinate system at each time t_i when $\omega t_i + \Theta_0 - (2\pi/\lambda)d = -\pi + 2\pi i$. Hence, the stimulating sequence will be generated as

$$I(t) = A\delta\left[\cos\left(\omega t - \pi + \Theta_0 - \frac{2\pi}{\lambda} d - \omega\tau\right) - 1\right], \tag{15}$$

with the phase shift ϕ_m determined by the following expression:

$$\phi_m = \pi - \Theta_0 + \frac{2\pi}{\lambda} d + \omega\tau. \tag{16}$$

To determine the direction of the drift induced by the one-channel feedback, expression (16) should be substituted into Eq. (14), which yields

$$\gamma = \varphi + \pi + \frac{2\pi}{\lambda} d + \omega\tau. \tag{17}$$

It is important to stress that under the described one-channel feedback, the drift direction does not depend on the initial orientation Θ_0 of the spiral. The displacement d of the spiral center from the detection point and the time delay τ completely determine the drift angle γ with respect to the displacement direction.

Along a resonant orbit around the detecting point, the induced drift is always orthogonal to the radial direction. This means that the drift angle γ should obey the simple condition

$$\gamma = \pi/2 + \pi n, \tag{18}$$

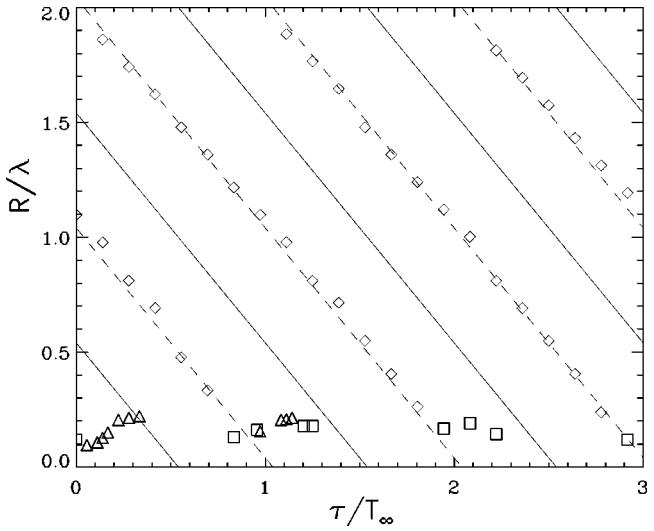

FIG. 9. Radius R of the resonance attractors vs the time delay τ computed for the Oregonator model (diamonds) and predicted by Eq. (19) (dashed lines). Boundaries of basins of attraction according to Eq. (20) are shown by solid lines. Radii of the entrainment and asynchronous attractors are shown by triangles and squares, respectively.

where n is an arbitrary integer. It follows from Eq. (17) that the motion along the circular pathway will be stable only if n is an even number: $n=2m$. Indeed, according to Eq. (17), γ increases with d. Therefore, small deviations from the circular pathway are damped out (amplified) for $n=2m$ $(n=2m+1)$. The radius R of the corresponding orbit can be found as a solution of Eqs. (17) and (18):

$$R/\lambda = m - 0.25 - \frac{\varphi}{2\pi} - \tau/T_\infty . \tag{19}$$

These stable orbits are the attractors of a spiral wave under the one-channel feedback. The basins of attraction are bounded by unstable orbits, which corresponds to $n=2m+1$, and have radii

$$R/\lambda = m + 0.25 - \frac{\varphi}{2\pi} - \tau/T_\infty . \tag{20}$$

In order to apply this theory to the Oregonator model, the characteristic constant φ should be determined. To this end, the computations presented in Fig. 3 can be used. Indeed, the orientation of the spiral wave just before the beginning of the periodic stimulation is shown in Fig. 3(a). The presented front shape is approximated by Eq. (13) with $\Theta_0=0.65$ and $\lambda=17.7$. The angle γ which specifies the drift direction shown in Fig. 3(b) is estimated as $\gamma=-1.15$. Taking into account that in these computations the phase shift $\phi_m=0$, and substituting these data into Eq. (14), the value $\varphi=-1.80$ is found.

Substitution of this value into Eq. (19) yields the attractor radius R as a function of the time delay τ in the feedback loop. This relationship is plotted as dashed lines in Fig. 9. For each value of τ, there are several possible stable orbits corresponding to different values of the integer m. The spiral wave is attracted to an orbit with a given m if initially it is located in the corresponding basin of attraction. The boundaries of the basin of attraction are determined by Eq. (20) and shown by solid lines in Fig. 9. These theoretical predictions are in good quantitative agreement with the results of the direct integration of the Oregonator model (12) represented by diamonds in Fig. 9.

Only in the region of small radii, where $R<0.3\lambda$, dependence (19) is violated. This is the region where the entrainment attractor can be observed. Radii of the entrainment attractors obtained in computations presented in Fig. 8 are also shown in Fig. 9. For small τ, the radius increases with the time delay and reaches the boundary of the basin of attraction of the resonance attractor at $\tau/T\approx 0.4$. This critical value for the time delay is shown as the left dotted line in Fig. 8. For larger time delay, within the basin of attraction of the resonance attractor, the entrainment attractor becomes unstable [cf. Figs. 7(a) and 7(b)]. The radius of the entrainment attractor remains nearly constant when the time delay increases and can be estimated as $R_e=0.2\lambda$. Using this estimate and considering Fig. 9, it can be expected that the entrainment attractor is unstable in the interval $0.4<\tau/T_\infty<0.9$ and the resonance attractor should be observed. This interval of τ is marked by a bar in Fig. 8.

Now it becomes clear why a branch of the period shift function with a negative slope was not found in our computations illustrated by Fig. 8. Indeed, the entrainment attractor cannot exist within the basin of attraction of the resonance attractor.

Expressions (19) and (20) and Fig. 9 show that the interval of τ, where only the resonance attractor can be observed, will appear periodically along the τ axis with period T_∞ (see other bars in Fig. 8). Hence, once more the entrainment attractor can be expected within the interval $0.9<\tau/T_\infty<1.4$. Our computations with $\tau/T_\infty\approx 1.0$ confirm this prediction as shown in Fig. 8. However, even in this interval of τ, where the resonance attractor does not destroy the synchronized motion, it was impossible to observe a branch of the period shift function with a negative slope. Instead of complete synchronization, the trajectory looks like an asynchronous motion, still occupying a relatively small spatial domain, as shown in Fig. 7(c). We call this new dynamical regime the asynchronous attractor.

Figure 8 shows that the next possible region of the entrainment attractor is located near $\tau/T_\infty\approx 2.0$. However, here also only the asynchronous attractors have been found, e.g., see Fig. 7(d).

V. THE BZ REACTION UNDER ONE-CHANNEL FEEDBACK

The experimental part of this work is performed with the light-sensitive version of the BZ reaction using the setup described in Ref. [18]. An open reactor allows us to maintain the system in a stationary nonequilibrium state. Premixed feeding solution prepared from stock solutions containing $[NaBrO_3]_0=(2.06\times 10^{-1})M$ (Aldrich, 99 +%), $[H_2SO_4]_0=(3.1\times 10^{-1})M$ (Aldrich, 95–98 %), malonic acid

$[CH_2(COOH)_2]_0=(1.86\times10^{-1})M$ (Aldrich, 99%), and $[NaBr]_0=4.12\times10^{-2}$ (Fluka, p.a.) is pumped continuously through the reactor with the rate 120 ml/h. Circulating water from a thermostat maintains the temperature at (25.0 ±0.5) °C. The catalyst is immobilized in a silicahydrogel layer of 0.5 mm thickness (active layer) prepared on a plate of frozen glass (diameter 63 mm). To protect the active layer from stirring effects, it is covered by an inactive gel layer not loaded with the catalyst.

The active layer is illuminated by a video projector (Panasonic PT-L555E) controlled by a computer via a frame grabber (Data Translation, DT 2851). The illuminating light is filtered with a bandpass filter (BG6, 310–530 nm). Every 1 s the pictures of the oxidation waves appearing in the gel layer are detected in transmitted light by a charge-coupled device camera (Sony AVC D7CE) and digitized with a frame grabber (Data Translation, DT 3155) for immediate processing by the computer. During the same time step, the light signal applied by the projector can be changed in accordance with the processed information (feedback) or following an *a priori* given program (e.g., periodic forcing).

A single spiral wave, which constitutes the initial condition for all the experiments, is created in the center of the gel disk by breaking a wave front with an intense light spot. The location of the spiral wave tip is defined online as the intersection point of contour lines (0.6× amplitude) extracted from two digitized images taken with time interval 2.0 s. The tip trajectory, the control signal, and the wave activity at an arbitrary detection point can be visualized online by the computer.

An unperturbed spiral has the wavelength $\lambda\approx2.0$ mm. Its tip describes a meandering trajectory containing about four lobes. The rotation period measured far away from the symmetry center was $T_\infty\approx40$ s.

Under a periodic change of the illumination, the spiral rotation can be synchronized. Figures 10(a) and 10(b) show two examples of such synchronized spiral tip motion observed for two different periods of external forcing. Simultaneous registration of the wave activity at the symmetry center of the observed trajectory allows us to measure the time delay between the wave passage through the center and the application of an external perturbation. These data are used to determine the period shift function shown in Fig. 11.

Application of the one-channel feedback control also allows us to observe a synchronized motion if the entrainment attractor is created. For instance, the tip trajectory shown in Fig. 10(b) is observed for both types of stimulation: periodic forcing and one-channel feedback control. However, not all synchronized regimes obtained under periodic forcing can be reproduced by application of the one-channel feedback and vice versa. For instance, the trajectory shown in Fig. 10(a) is observed only in experiments with periodic forcing. All attempts to reproduce the periodic regime introducing a corresponding time delay into the feedback loop resulted in a resonance attractor. On the other hand, a periodic forcing does not synchronize the spiral tip motion in the period range $0.88<T/T_\infty<0.93$, while a one-channel feedback does.

Another possible regime under the one-channel feedback control is the resonance attractor. An example of this regime

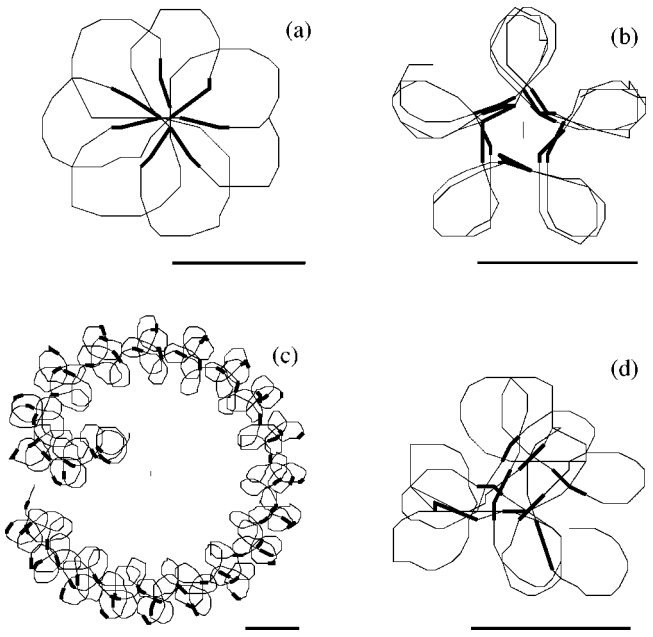

FIG. 10. Trajectories of the spiral wave tip observed in experiments with the BZ reaction under periodic forcing (a), (b) and under the one-channel feedback (b)–(d). (a) $T=28$ s, $\tau=22$ s; (b) $T=32$ s, $\tau=0$ s; (c) $\tau=4$ s; (d) $\tau=30$ s. Thick segments of the trajectory correspond to the application of the external impulses. Scale bar: 0.5 mm.

is shown in Fig. 10(c). In contrast to the entrainment attractor, the rotation center moves along a circle with a radius much larger than the size of single lobes. This radius depends on the time delay τ in the feedback loop. Data of a systematic study of this dependence are shown in Fig. 12 by diamonds.

The asynchronous attractor is also observed in our experi-

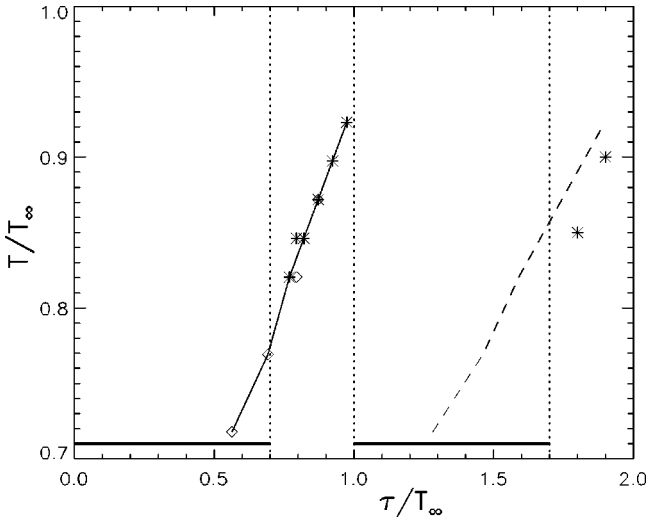

FIG. 11. Period shift function corresponding to periodic forcing (diamonds) and one-channel feedback (asterisks) obtained experimentally for the light-sensitive BZ medium (solid line). Extrapolation to larger values of τ is shown by the dashed line. Within intervals of τ bounded by dotted lines and marked by horizontal bars, the resonance attractors are observed.

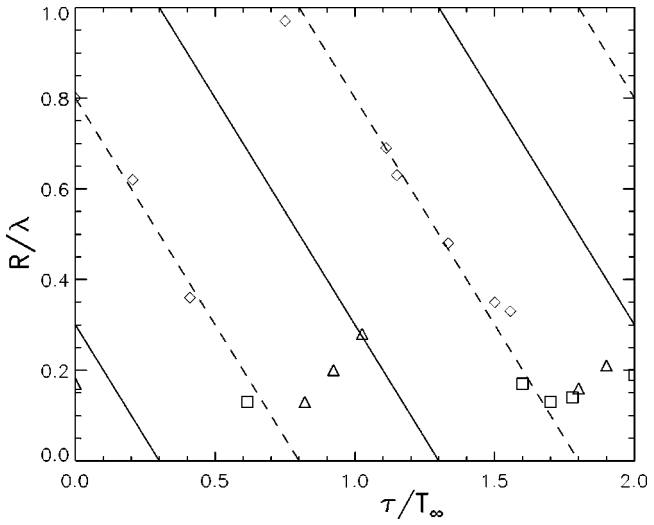

FIG. 12. Radii of resonance (diamonds), entrainment (triangles), and asynchronous (squares) attractors determined experimentally for meandering spiral waves in the light-sensitive BZ medium vs the time delay in the feedback loop. The dashed lines show the theoretical predictions for the radii of the resonance attractor according to Eq. (19), the solid lines are the boundaries of the basins of attraction according to Eq. (20).

ments [e.g., see Fig. 10(d)]. In contrast to the resonance attractor, the motion of the spiral tip is restricted to a relatively small spatial domain, such as in the case of the entrainment attractor. However, this motion is not synchronized with the feedback signal.

Expression (19) for the radius of the resonance attractor contains only one unknown parameter φ, which specifies the direction of the resonance drift. In order to avoid rather complicated experimental procedure to determine this value, the obtained experimental data were fitted by linear dependences (19) with $\varphi = -0.31$ as shown in Fig. 12 by dashed lines. Then, the boundaries of the basin of attraction were specified in accordance with Eq. (20) (solid lines in Fig. 12). These basins of attraction determine intervals of the time delay τ corresponding to the appearance of the resonance attractor. These intervals are marked by horizontal bars and vertical dotted lines in Fig. 11.

VI. DISCUSSION

A systematic study of the meandering spiral wave under pulsatory modulation performed in this work demonstrates very reach diversity of possible dynamical regimes. To identify relationships in this diversity, a comparison between periodic forcing and feedback control is shown to be very useful.

In this work, the Poincaré oscillator is considered in order to demonstrate the advantages of this comparison based on the application of the period shift function. In contrast to the phase transition curve (that is frequently applied in the study of periodically forced nonlinear oscillators [2,3,23]), the period shift function is used quite rarely. However, there are some studies where this function has been measured [30,31], while the term itself was proposed independently in Ref. [24]. For lumped systems, the period shift function is very helpful to analyze the stability of a frequency locked motion and bistability phenomena.

The motion of a meandering spiral wave under fixed phase feedback control in many aspects resembles the dynamics of a periodically perturbed nonlinear lumped oscillator. Indeed, the period shift functions shown in Figs. 1(b) and 6 are qualitatively identical. Frequency locked oscillations take place in a restricted range of the forcing period. Only the part of the period shift function with positive slope is reproducible under periodic forcing. For sufficiently large time delay in the feedback loop, bistability can be observed.

Apart from a fixed phase control, there are many other possibilities to construct an effective feedback mechanism in an excitable medium. A typical example is a one-channel feedback that is analyzed in detail in this work. This type of feedback control is commonly used in experiments with the BZ reaction [11–13,18,19] and induces qualitatively new features in the dynamics of meandering spiral waves compared to lumped oscillators. Our systematic study of spiral wave dynamics under the one-channel feedback reveals three types of attractors of meandering spiral waves. Two of them, the resonance and the entrainment attractors, have been reported earlier [11,12], while the third one, the asynchronous attractor, was unknown. The final diagram in Fig. 12 shows the mutual arrangement of these three types of attractors. Among them the most surprising is the resonance attractor, which appears as characteristic features of distributed systems. In contrast to the frequency locked motion of lumped oscillators, a temporal synchronization is not a specific property of this regime. Nevertheless, the resulting trajectories are well ordered in space [see Figs. 3(b) and 7(b)].

In this work, the theory of the resonance attractor developed earlier for a rigidly rotating spiral [17,21] is generalized to the case of meandering spiral waves. The obtained dependence (19) of the attractor radius on the time delay in the feedback loop contains only one unknown parameter, which can be directly measured or determined from available experimental data. The resulting theoretical predictions for the attractor radius are in good quantitative agreement with both numerical and experimental data (cf. Figs. 9 and 12).

Our theory predicts also the basins of attraction (solid lines in Figs. 9 and 12) and allows us to answer the important question first posed in Ref. [12]: Why does the entrainment attractor become unstable for sufficiently large time delay? Our study clearly demonstrates that this destabilization takes place if the spiral tip enters into the basin of attraction of a resonance attractor.

The intervals of the time delay corresponding to the resonance attractors are marked by bars in Figs. 8 and 9. Within these intervals, the spiral core tends to describe a long excursion around the detection point. Outside these intervals, the estimated radius of the resonance attractor is smaller than the size of the entrainment attractor. Hence, the spiral tip should always remain in the vicinity of the detecting point. If this restricted motion is synchronized with external forcing, the entrainment attractor is observed. Otherwise, the asynchronous attractor appears. In order to predict intervals of τ where the entrainment attractor is expected, the period shift

function obtained for small values of the time delay is extrapolated to a broader range of τ (see Figs. 8 and 11) similar to what can be done in the case of a lumped oscillator.

The asynchronous attractor observed in our experiments and computations exhibits irregular dynamics of an excitable medium in a parameter region which is far away from the hypermeandering limit discovered by Winfree [32]. Irregular behavior appears here as a consequence of an instability of the entrainment attractor induced by the applied one-channel feedback control. It is known that similar instabilities of feedback-controlled oscillations can also be observed in the case of lumped oscillators [see, e.g., Fig. 2(b)] and corresponding stability conditions can be derived [e.g., Eq. (11) in the case of the Poincaré oscillator]. The determination of exact conditions for the transition between entrainment and asynchronous attractors remains as a challenge to future investigations.

Thus, while fixed phase feedback control leads to results which are very similar to those observed for a lumped oscillator, the one-channel feedback control reveals very specific properties of a distributed system, which are obtained numerically, observed experimentally, and explained theoretically. In particular, the main features of the diagrams in Figs. 9 and 12 summarizing the experimental and numerical data can be explained in the framework of the developed theory. As a continuation of this work, it will be interesting and important to analyze the dynamics of meandering spiral waves subjected to a global feedback control, studied till now only in application to rigidly rotating spiral waves [33,22].

ACKNOWLEDGMENT

The authors thank the Deutsche Forschungsgemeinschaft (DFG, Grant No. SFB 555) for financial support.

[1] V.I. Arnold, *Geometrical Methods in the Theory of Ordinary Differential Equations* (Springer, Berlin, 1988).
[2] Y. Kuramoto, *Chemical Oscillations, Waves and Turbulence* (Springer, Berlin, 1984).
[3] A.T. Winfree, *The Geometry of Biological Time* (Springer, Berlin, 2000).
[4] S.K. Scott, *Chemical Chaos* (Clarendon Press, Oxford, 1991).
[5] J. Keener and J. Sneyd, *Mathematical Physiology* (Springer, Berlin, 1998).
[6] A. Pikovsky, M. Rosenblum, and J. Kurths, *Synchronization* (Cambridge University Press, Cambridge, 2001).
[7] O. Steinbock, V.S. Zykov, and S.C. Müller, Nature (London) **366**, 322 (1993).
[8] M. Braune and H. Engel, Chem. Phys. Lett. **211**, 534 (1993).
[9] V.S. Zykov, O. Steinbock, and S.C. Müller, Chaos **4**, 509 (1994).
[10] A. Schrader, M. Braune, and H. Engel, Phys. Rev. E **52**, 98 (1995).
[11] S. Grill, V.S. Zykov, and S.C. Müller, Phys. Rev. Lett. **75**, 3368 (1995).
[12] S. Grill, V.S. Zykov, and S.C. Müller, J. Phys. Chem. **100**, 19082 (1996).
[13] V.N. Biktashev and A. Holden, J. Theor. Biol. **169**, 101 (1994).
[14] A.V. Panfilov, S.C. Müller, V.S. Zykov, and J.P. Keener, Phys. Rev. E **61**, 4644 (2000).
[15] V.A. Davydov, V.S. Zykov, and A.S. Mikhailov, Usp. Fiz. Nauk **161**, 45 (1991) [Sov. Phys. Usp. **34**, 665 (1991)].
[16] R.M. Mantel and D. Barkley, Phys. Rev. E **54**, 4791 (1996).
[17] A. Karma and V.S. Zykov, Phys. Rev. Lett. **83**, 2453 (1999).
[18] M. Braune and H. Engel, Phys. Rev. E **62**, 5986 (2000).
[19] O.U. Kheowan, V.S. Zykov, O. Rangsiman, and S.C. Müller, Phys. Rev. Lett. **86**, 2170 (2001).
[20] M. Hildebrand, H. Skodt, and K. Showalter, Phys. Rev. Lett. **87**, 088303 (2001).
[21] V.S. Zykov, O.U. Kheowan, O. Rangsiman, and S.C. Müller, Phys. Rev. E **65**, 026206 (2002).
[22] V.S. Zykov and H. Engel, Phys. Rev. E **66**, 016206 (2002).
[23] L. Glass and M.C. Mackey, *From Clocks to Chaos* (Princeton University Press, Princeton, NJ, 1988).
[24] W. Vance and J. Ross, J. Chem. Phys. **103**, 2472 (1995).
[25] L. Glass and W.Z. Zeng, Ann. N.Y. Acad. Sci. **591**, 316 (1990).
[26] S.C. Müller, T. Plesser, and B. Hess, Science **230**, 661 (1985).
[27] G.S. Skinner and H.L. Swinney, Physica D **48**, 1 (1991).
[28] *Chemical Waves and Patterns*, edited by R. Kapral and K. Showalter (Kluwer, Dordrecht, 1995).
[29] H.-J. Krug, L. Pohlmann, and L. Kuhnert, J. Phys. Chem. **94**, 4862 (1990).
[30] J. Weiner, F.W. Schneider, and K. Bar-Eli, J. Phys. Chem. **93**, 2704 (1989).
[31] M. Pollman, M. Bertram, and H.H. Rotermund, Chem. Phys. Lett. **346**, 123 (2001).
[32] A.T. Winfree, Chaos **1**, 303 (1991).
[33] V.S. Zykov, A.S. Mikhailov, and S.C. Müller, Phys. Rev. Lett. **78**, 3398 (1997).